Asymmetric Gramicidin Channels: Heterodimeric Channels with a Single F_6Val[1] Residue

Shigetoshi Oiki,*§ Roger E. Koeppe II,‡ and Olaf S. Andersen*

*Department of Physiology and Biophysics, Cornell University Medical College, New York, New York 10021 USA, ‡Department of Chemistry and Biochemistry, University of Arkansas, Fayetteville, Arkansas 72701 USA, and §Department of Cellular and Molecular Physiology, National Institute for Physiological Sciences, Myodaiji, Okazaki 444 Japan

ABSTRACT Substitution of Val[1] by 4,4,4,4′,4′,4′-F_6Val in [Val[1]]gramicidin A ([Val[1]]gA) produces channels in which the effects of amino acid replacements on dimer stability and ion permeation are nonadditive. If only one Val[1] (in a symmetric [Val[1]]gA channel) is substituted by F_6Val, the resulting heterodimeric channels are destabilized relative to both homodimeric parent channels and the single-channel conductance of the heterodimeric channels is reduced relative to the parent channels (Russell, E. W. B., L. B. Weiss, F. I. Navetta, R. E. Koeppe II, and O. S. Andersen. 1986. Single-channel studies on linear gramicidins with altered amino acid side chains. Effects of altering the polarity of the side chain at position #1 in gramicidin A. *Biophys. J.* 49:673; Durkin, J. T., R. E. Koeppe II, and O. S. Andersen. 1990. Energetics of gramicidin hybrid channel formation as a test for structural equivalence. Side-chain substitutions in the native sequence. *J. Mol. Biol.* 211:221–234). To understand the basis for this destabilization, we have examined further the characteristics of [F_6Val[1]]/[Xxx[1]]gA heterodimers, where Xxx = Gly, Val, and Ala. These heterodimeric channels show rapid current transitions between (at least) two current levels and display asymmetric *i-V* characteristics. The orientation of the heterodimers relative to the applied potential was determined by asymmetric addition of the gramicidin analogs, one to each side of a preformed bilayer. The current transitions are most clearly illustrated for [F_6Val[1]]/[Gly[1]]gA heterodimers, which possess two finite and well defined current levels. Based on the existence of these two conductance states and the analysis of duration and interval distributions, we conclude that the transitions between the two current levels correspond to conformational transitions in "stable" heterodimers. In the case of [F_6Val[1]]/[Val[1]]gA and [F_6Val[1]]/[Ala[1]]gA heterodimers, the low-conductance state is indistinguishable from zero. The two (or more) conductance states presumably correspond to different orientations of the dipolar F_6Val[1] side chain. The distribution between the high- and the low-conductance states varies as a function of potential in [F_6Val[1]]/[Gly[1]]gA channels. These characteristics cause the [F_6Val[1]]/nonpolar (Val, Ala, Gly)gA hybrid channels to serve as a "simple" model for understanding gating transitions in membrane-spanning channels.

INTRODUCTION

Gramicidin channels are extensively used to investigate the structure-function relations of ion permeation, peptide-peptide interactions, and peptide-lipid interactions of membrane channels (e.g., Andersen et al., 1992; Andersen and Koeppe, 1992; Killian, 1992; Busath, 1993). The linear gramicidin A (gA) has the sequence (Sarges and Witkop, 1965): Formyl-L-Val[1]-Gly[2]-l-Ala[3]-D-Leu[4]-L-Ala[5]-D-Val[6]-L-Val[7]-D-Val[8]-L-Trp[9]-D-Leu[10]-L-Trp[11]-D-Leu[12]-L-Trp[13]-D-Leu[14]-L-Trp[15]-ethanolamine. The channels are dimers of $\beta^{6.3}$-helices, in which the formyl-NH-termini of the monomers associate via six hydrogen bonds to create a C_2 symmetric dimer with an axis of symmetry that is perpendicular to the pore axis. This structural symmetry is reflected in channel function as symmetric single-channel current-voltage (*i-V*) characteristics, which are observed also with channels formed by any side chain-substituted gramicidin analog—as long as the channels are homodimers (being formed by identical monomers). When amino acid substitutions are introduced into only one monomer, the channels become asymmetric heterodimers, which generally is reflected in channel function as asymmetric (rectifying) *i-V* characteristics (Veatch and Stryer, 1977; Apell et al., 1977; Mazet et al., 1984; Russell et al., 1986; Andersen et al., 1988; Durkin et al., 1990; Becker et al., 1991; Fonseca et al., 1992) and as polarity-dependent dimer durations (Koeppe et al., 1992; Fonseca et al., 1992). The structure and function of gramicidin channels thus preserve a consistent relation with respect to symmetry.

Taking the [Val[1]]gA homodimer as the reference or "wild-type" channel, heterodimers formed between [Val[1]]gA and a sequence-substituted gramicidin analog correspond to singly-substituted channels, whereas homodimers formed by the analog correspond to doubly-substituted channels. These different channel types are seen when [Val[1]]gA and the analog in question both are added to both sides of a bilayer. For analogs with nonpolar or dipolar substitutions at position #1, the heterodimeric (hybrid) channels usually have characteristics that are intermediate to those of the homodimeric channels (e.g., Durkin et al., 1990). That is, the conductance and duration changes that are caused by a single dipolar substitution are usually enhanced by the double substitution. For such cases, the substitutions exert additive[1] effects on the conductance and duration changes. There are exceptions to this rule.

Received for publication 23 June 1993 and in final form 1 February 1994.

Address reprint requests to Olaf S. Andersen, Department of Physiology and Biophysics, Cornell University Medical College, 1300 York Avenue, New York, NY 10021-4896. Tel.: 212-746-6350; Fax: 212-746-8690; E-mail: sparre@med.cornell.edu.

0006-3495/94/06/1823/10 $2.00

[1] More precisely, the energetic changes are additive; the functional changes will be multiplicative.

A "mutant" gramicidin in which the Val at position #1 is substituted by 4,4,4,4′,4′,4′-F_6-Val ([F_6Val^1]gA), for example, forms hybrid channels with [Val^1]gA (Russell et al., 1986). But the conductance of the [F_6Val^1]/[Val^1]gA hybrid channels is *less* than the conductance of either parent homodimer. Moreover, the average duration of the hybrid channels is also *less* than that of both parent homodimers (Russell et al., 1986). The conductance and duration changes produced by single and double substitutions, therefore, are not additive. In fact, measurements of the energetics of heterodimer formation and stability show that the [F_6Val^1]gA/[Val^1]gA heterodimers are destabilized relative to the parent homodimers (Durkin et al., 1990). The F_6Val residue thus violates the "simple" additivity rule.

There is another paradox. Even at 300 mV, there is only one hybrid channel peak in current transition amplitude histograms for [F_6Val^1]/[Val^1]gA channels, which is suggestive of a (nearly) symmetric *i-V* relation (cf. Russell et al., 1986). This is surprising, because the F_6Val side chain has a significant dipole moment (the moments along the C_α-C_β axis and in the C_β-C_γ-$C_{\gamma'}$ plane (bisecting the β-γ-γ' angle) are ~1.6 Debye (cf. Russell et al., 1986)); and experiments with other dipolar substitutions at this position, near the channel center, indicate that the two heterodimer orientations should be distinguishable (Russell et al., 1986; Andersen et al., 1988).

To examine further the effect of the F_6Val residue on gramicidin channel function, we made use of the channels' dimeric nature to "express" various heterodimers by adding different combinations of analogs to one or both sides of the bilayer. We began in an heuristic way: if the F_6Val residue poses steric constraints on its host monomer, the introduction of additional flexibility into the opposite monomer might help to relieve strain at the dimer junction and thus reconcile the two monomers. The #2 residue is Gly, and the introduction of an additional Gly at position #1 should impart an increased flexibility to the peptide backbone of that monomer, which could serve as a mechanical "buffer" at the dimer join. Surprisingly, we found that [F_6Val^1]/[Gly^1]gA heterodimers were multi-state channels with properties that depend on the polarity of the applied potential. In this article we describe the basic hybrid channel properties in planar bilayers and determine the heterodimer orientation. A brief description of the gating behavior has appeared (Oiki et al., 1992).

MATERIALS AND METHODS

The position #1-substituted gramicidins were synthesized and purified as previously described (Weiss and Koeppe, 1985; Russell et al., 1986; Durkin et al., 1990). F_6Val was purchased from Fairfield Chemical Co. (Blythewood, SC) as a mixture of D- and L-F_6Val. The enantiomers were not separated because experiments with other analogs ([Val^1]gA and [Phe^1]gA) suggest that the analog with the D-enantiomer is inert. We used the bilayer punch method (Andersen, 1983) to record single channel currents in symmetric unbuffered 1.0 M CsCl. Briefly, purified diphytanoylphosphatidylcholine (Avanti Polar Lipids, Pine Bluffs, AL) dissolved in *n*-decane (20 mg/ml) was used to form "large" membranes (~1.6 mm diameter). Small membranes (diameter ~30 μm) were isolated using silanized glass pipettes.

Single-channel current transitions were recorded with a Dagan 3900 patch clamp with a 3910 expander box (Dagan Instruments, Minneapolis, MN) at 25°C using three different protocols: i) adding single gramicidin analogs to both aqueous solutions (symmetric single addition); ii) adding two different analogs together to both solutions (symmetric dual addition); and iii) adding two different analogs, one to each side of a preformed membrane (asymmetric addition). In such experiments, one can maintain an almost complete asymmetric distribution of the two analogs for a surprisingly long time (>30 min), because position #1-substituted gramicidin A analogs cross lipid bilayers very slowly (O'Connell et al., 1990). One will always observe a few symmetric channels; but their frequency is only ~1% of the activity observed after asymmetric addition of the analog in question (O'Connell et al., 1990). The bilayer thus serves as an effective barrier against the free admixture of the added gramicidins between the two compartments. The transfer of gramicidins across the bilayer was monitored by following the pattern of channel appearances as a function of time.

The single-channel currents were recorded on VCR tape through a modified PCM amplifier (DAS 900, Unitrade/Dagan Corp.). The recorded data were played back through an 8-pole Bessel low-pass filter at 500 Hz (−3 dB point) and digitized at 2.5 kHz. Data acquisition and analysis were done using pClamp v. 5.5 (Axon Instruments, Foster City, CA). The dead-time in the analysis was ~0.4 ms.

RESULTS

[Gly^1]/[F_6Val^1]gA hybrid channels

Fig. 1 shows examples of single-channel currents arising from the four possible combinations of the two gramicidin analogs [Gly^1]gA and [F_6Val^1]gA. Symmetric addition of [Gly^1]gA (Fig. 1 *A*) produced channels with a conductance of 35 pS (in 1.0 M CsCl), which represent the symmetric (homodimeric) [Gly^1]gA channels. The single-channel conductance of the homodimeric [F_6Val^1]gA channels is 24 pS (Fig. 1 *B*). The average duration (τ) of the [F_6Val^1]gA homodimer, ~90 ms, is less than that of the [Gly^1]gA homodimer, ~130 ms (results not shown).

When [Gly^1]gA and [F_6Val^1]gA both are added to both sides of the bilayer, two new types of channels appear (Fig. 1 *C*), in addition to the two homodimers (where the latter are denoted "F" and "G"). These asymmetric channels are heterodimers, formed between one [F_6Val^1]gA and one [Gly^1]gA, and they have properties that are quite different from those of the symmetric channels: the average [F_6Val^1]gA/[Gly^1]gA heterodimer durations are much less than those of either of the homodimers, and there are rapid transitions between two current levels. These new channels are displayed in more detail (at a fivefold expanded time scale) in the current trace segments in Fig. 1 *D*.

The two hybrid channel types can be distinguished by their basal and maximal current levels. One type (denoted "*hh*") appears as "bursts of openings" to a high-conductance level that is very similar to that of symmetrical [F_6Val^1]gA channels and has a basal current level that is only slightly above the background current through the bilayer itself. The other hybrid channel type (denoted "*hl*") exhibits rapid transitions between two different current levels: a high-conductance level that is less than that of symmetrical [F_6Val^1]gA channels and a well defined "sub-conductance state" that is easily resolved even at this low resolution.

The two hybrid channel types correspond to the two opposite orientations of the heterodimer with respect to the

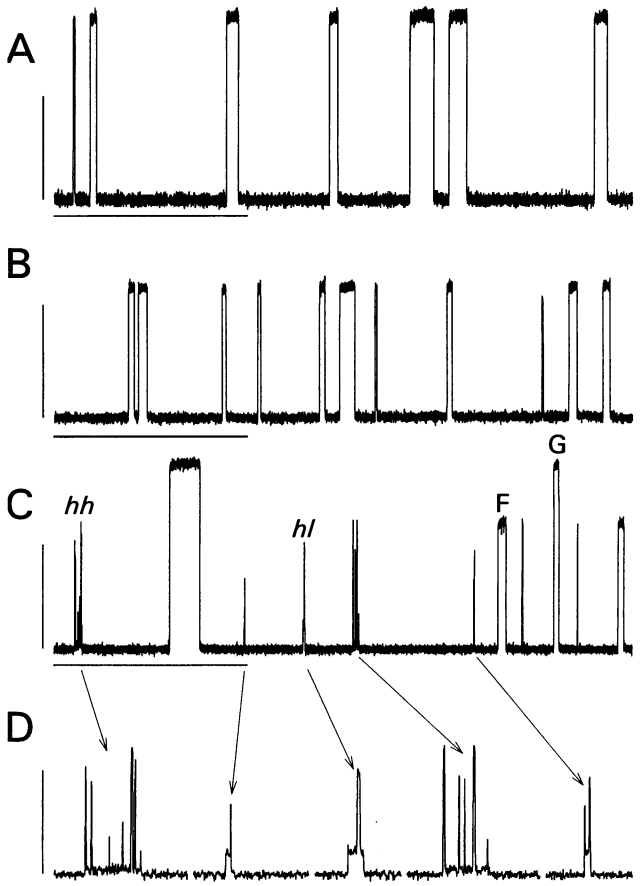

FIGURE 1 Single-channel current records obtained with either [Gly^1]gA or [F_6Val^1]gA and with their mixture. (*A*) Single-channel events seen after symmetric addition of [Gly^1]gA (symmetric [Gly^1]gA channels). (*B*) Single-channel events seen after symmetric addition of [F_6Val^1]gA (symmetric [F_6Val^1]gA channels). (*C*) Single-channel events seen after symmetric addition of both gramicidin analogs, which shows the two symmetrical channel types, labeled "F" ([F_6Val^1]gA channels) and "G" ([Gly^1]gA channels), as well as two new channel types, labeled *hl* and *hh*, which are [F_6Val^1]/[Gly^1]gA heterodimers. These new channel types are shown in more detail at a 7.5-fold expanded time scale in *D*. Calibration bars: vertically, 5 pA; horizontally (*A–C*), 2 s, (*D*) 0.4 s. 300 mV.

applied potential. This was shown in experiments with asymmetric addition of [Gly^1]gA and [F_6Val^1]gA to a preformed bilayer (Fig. 2), which allows one to define the orientation of the heterodimers in the bilayer because gramicidin A analogs cross lipid bilayers very slowly (O'Connell et al., 1990).[2] At positive potentials (which we define to be when the current, the net Cs^+ flux, is in the [Gly^1]gA174 [F_6Val^1]gA direction), one observes the *hl* channel type, which has a maximal current level that is less than that of the

[2] One of the hybrid channel types has a single-channel conductance that is similar to that of [F_6Val^1]gA channels (Fig. 1), and the experiments could be biased by the inadvertent inclusion of symmetrical [F_6Val^1]gA channels in the analysis. We guard against the transfer of [F_6Val^1]gA across the bilayer by monitoring the pattern of channel appearances at the polarity where the [F_6Val^1]gA/[Gly^1]gA heterodimers have a conductance that is clearly different from that of symmetrical [F_6Val^1]gA channels.

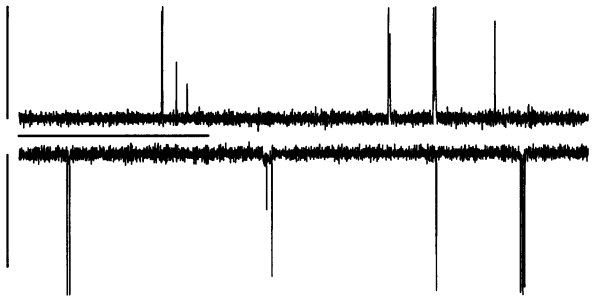

FIGURE 2 [F_6Val^1]/[Gly^1]gA heterodimers at different polarities. [Gly^1]gA was added to the *cis* solution and [F_6Val^1]gA was added to the *trans* solution, which is the electrical reference. The upper current trace was recorded at +300 mV, which we generally define to be when the current is in the [Gly^1]gA→[F_6Val^1]gA direction; one sees *hl* events. The lower current trace was recorded at −300 mV, when the current is in the opposite direction; one sees *hh* events. (The current transitions are not clearly seen at this relative poor time resolution, but the different peak current levels are clearly seen.) Calibration bars: vertically, 5 pA; horizontally, 1 s.

symmetrical [F_6Val^1]gA and a well defined substate (Fig. 2, *top*). (The substate is not well resolved here, because the traces are shown at a relatively low time resolution; higher-resolution traces are shown in Fig. 3.) At negative potentials (when the current is in the [F_6Val^1]gA→ [Gly^1]gA direction), one observes the *hh* channel type (Fig. 2, *bottom*).

The two-state behavior of *hl* and *hh* channels is seen more clearly in current traces at higher (time) resolution (Fig. 3). At both polarities one observes two well defined current levels, denoted as **H** (high-conductance) and **L** (low-conductance). (The two current levels are indicated by interrupted horizontal lines in Fig. 3, *A* and *C*.) The two current levels correspond to two different channel (dimer) states, because at either polarity the current level in the **L** state is significantly above the background current, which implies that the dimer remains intact in the **L** state. That is, an **H**↔**L** transition represents a well defined conformational change within a "stable" dimer rather than trains of successive monomer↔dimer events. One can assign, therefore, an (overall) duration to the dimer from the current traces: see, for example, the two successive dimer formation events separated by a short interruption in the first current segment of Fig. 3 *C*.

This conclusion, that the **H**↔**L** transitions represent conformational transitions in an intact dimer, was verified by analysis of the duration distributions for the *hh* events (Fig. 4) and *hl* events (Fig. 5). The results are shown using a logarithmic time axis (Sigworth and Sine, 1987). For either channel type (*hl* and *hh*), the durations were determined in two different ways. First (Figs. 4 *A* and 5 *A*), the dimer durations were determined as the time *from* a current transition originating at the baseline (bare bilayer) to either the **H** or the **L** current level *to* the first transition that returns to the baseline. The dimer intervals (Figs. 4 *B* and 5 *B*) were correspondingly determined as the time *from* a transition to the baseline *to* the next current transition to either the **H** or the **L** state. Second, the **H** state durations (Figs. 4 *C* and 5 *C*) were determined as the time *from* a current transition originating at either the

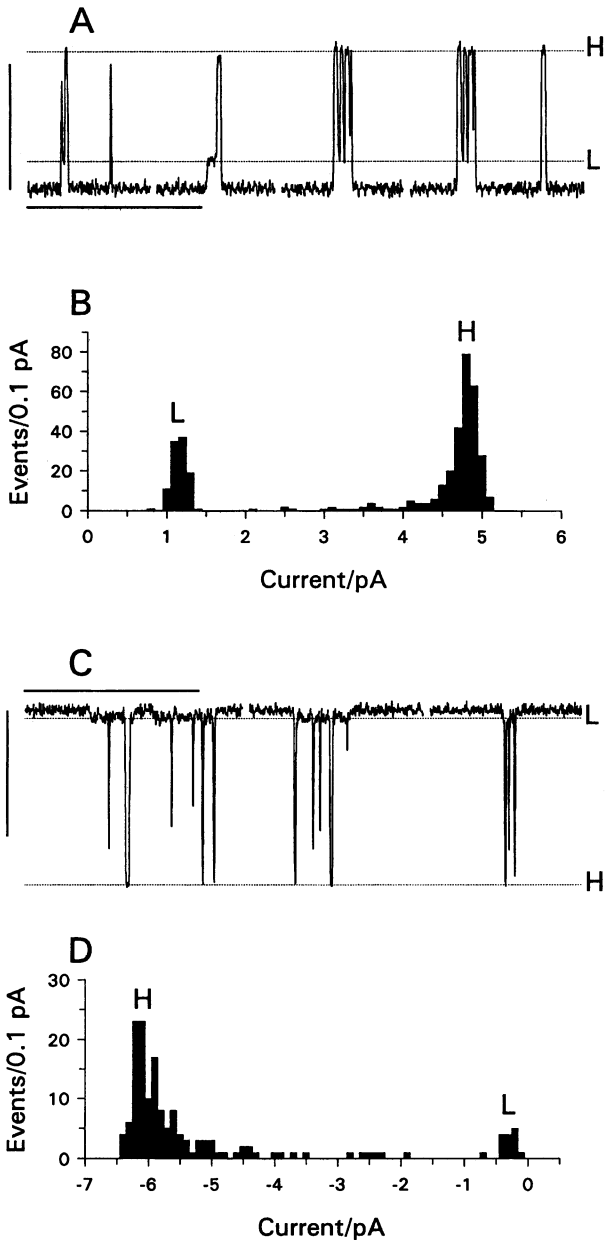

FIGURE 3 [F_6Val^1]/[Gly^1]gA hybrid channels at higher resolution. (*A*) *hl* single-channel events at positive potentials (sign convention as in Fig. 2). (To show the channels' fine structure, we show only selected current trace segments.) The two horizontal stippled lines, labeled **L** and **H**, denote the current level for the **L** and **H** states determined from current level histograms (shown in *B*). Calibration bars: vertically, 5 pA; horizontally, 200 ms. (*B*) current amplitude histograms, the peaks corresponding to the **H** and **L** states are so labeled. (*C*) *hh* single-channel events at negative potentials. The horizontal stippled lines have the same significance as in *A*. Calibration bars as in *A*. (*D*) current amplitude histograms, the peaks corresponding to the **H** and **L** states are so labeled. The "tail" in the **H** peak is due to limited time resolution.

L state or the baseline to the **H** state *to* the next current transition back to either the **L** state or the baseline; and the **H** intervals (Figs. 4 *D* and 5 *D*) were determined as the time *from* a current transition from the **H** state to either the **L** state or the baseline *to* the next transition to the **H** state. (Dimer durations and intervals were determined by setting the threshold levels between the baseline and the **L** state current levels; the **H** durations and intervals were determined by setting the threshold levels between the **L** and the **H** state current levels.)

At either polarity, the dimer duration histograms (Figs. 4 *A* and 5*A*) could be described as the sum of two exponential components, whereas the dimer interval histograms (Figs. 4 *B* and 5 *B*) could be described by only a single exponential distribution. In this analysis, the **H** and **L** states are lumped together, and there should be (at least) two exponential terms in the dimer duration distributions, whereas there should be only a single type of intervals (the "no dimer" state) and, therefore, only a single exponential term in the interval distribution. In contrast, the **H** state duration histograms (Figs. 4 *C* and 5 *C*) could be described using a single exponential distribution, whereas there was a new short-lived component in the **H**-state interval histograms (Figs. 4 *D* and 5 *D*). The new component in the interval distribution provides evidence for the existence of two different types of non-**H** states (the **L** state and the no-dimer state). The **H**↔**L** current transitions thus denote conformational transitions within a (stable) [F_6Val^1]gA/[Gly^1]gA heterodimer.

The average dimer durations ($\tau_{av} = (\sum_{i=1}^{n} t_i/n$, where t_i is the duration of event i and n is the total number of events) vary as a function of polarity: at − 300 mV (i.e., for the *hh* channels), $\tau_{av} \approx 13$ ms; at +300 mV (i.e., for the *hl* channels), $\tau_{av} \approx 6$ ms. The probability of being in the **H** state ($p_H = (\sum_{i=1}^{m} t_i^H)/(\sum_{i=1}^{n} t_i^D)$, where the superscripts "H" and "D" denote the **H** state and total dimer durations, respectively, while n and m denote the total number of each type of event) is likewise a function of the applied potential: $p_H(-300) \approx 0.3$ and $p_H(+300) \approx 0.5$. These channels thus possess (weakly) voltage-dependent properties (see also Oiki et al., 1992).

Based on current transition histograms at both polarities (Fig. 3), the **H**-state conductance is higher at negative potentials, whereas the **L**-state conductance is higher at positive potentials. The rectification of the **H** state (determined as $i_H(+300)/i_H(-300) \approx 0.8$) is more pronounced than for most hybrid channels with a dipolar position ≠1 substitution (cf. Table 2 of Durkin et al., 1990). Assuming that the **L** state at the two polarities corresponds to the same channel state, the magnitude of rectification of the **L** state is even greater than for the **H** state ($i_L(+300)/i_L(-300) \approx 6$), but in the opposite direction. (The degree of rectification is increased as $i(+300)/i(-300)$ either decreases below or increases above 1.0.)

[Val^1]/[F_6Val^1]gA hybrid channels

The prominent asymmetry observed with [F_6Val^1]-/[Gly^1]gA hybrid channels, with respect to both *i-V* rectification and dimer stability, suggests that [F_6Val^1]/[Val^1]gA hybrid channels have a similar asymmetry. This could account for the original observation (Russell et al., 1986) of only a single hybrid channel type. Indeed, that turns out to be the case. As with [F_6Val^1]/[Gly^1]gA heterodimers, one

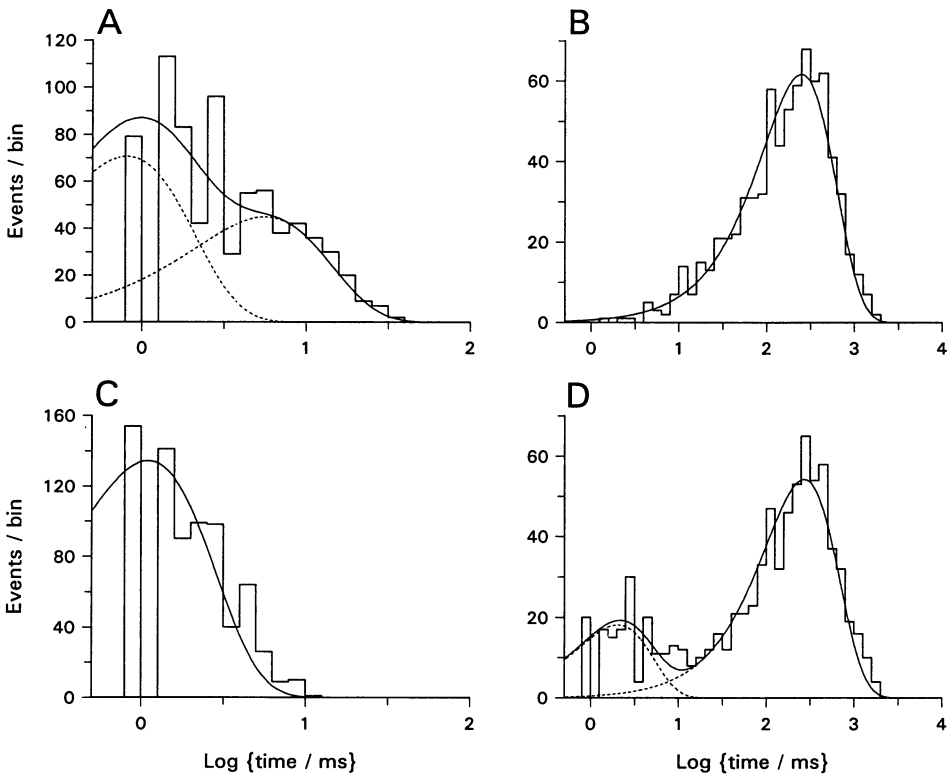

FIGURE 4 Duration distributions for the *hl* events. (*A*) Dimer duration distribution. The solid curve shows the least-squares fit obtained when fitting the results by the sum of two exponential distributions; the two interrupted curves show the two distributions. The slow and fast time constants and relative fractions, respectively, of events are: 0.9 ms and 0.6; and 6.3 ms and 0.4. (*B*) The corresponding dimer interval distribution. The solid curve shows the least-squares fit obtained when fitting the results by a single exponential distributions. The time constant is 280 ms. (*C*) Durations of the **H** state only. The solid curve shows the least-squares fit obtained when fitting the results by a single exponential distribution. The time constant is 1.2 ms. (*D*) The corresponding interval distribution for the **H**-state events. The solid curve shows the least-squares fit obtained when fitting the results by the sum of two exponential distributions; the two interrupted curves show the two distributions. The slow and fast time constants and relative fractions, respectively, of events are: 2.3 ms and 0.25; and 300 ms and 0.75.

can observe two hybrid channel types with [F_6Val^1]gA and [Val^1]gA. In Fig. 6 *A*, a low-conductance hybrid channel type (denoted *hl*) is relatively easy to distinguish from the two symmetric channel types (denoted "F" and "V"). The other hybrid channel type (denoted *hh*) appears as brief bursts to a current level that is similar to the current level for symmetrical [F_6Val^1]gA channels.

That these bursting events correspond to hybrid channels was shown in experiments where the two analogs were added asymmetrically, only one to each side (Fig. 6 *B*). At positive potentials (+300 mV), when the current is in the [Val^1]-gA→[F_6Val^1]gA direction, one sees the *hl* channels with a single-channel current of ~4.5 pA, which is less than the current through symmetric [F_6Val^1]gA channels (~7.0 pA). This is the hybrid channel type that was recognized by Russell et al. (1986). At negative potentials one sees the *hh* channels, with a conductance that is indistinguishable from that of the symmetric [F_6Val^1]gA channels. But this channel type is not a [F_6Val^1]gA homodimer because the average duration of the conducting events is much less (~1 ms, see Fig. 7 *C*) than that of symmetric [F_6Val^1]gA channels (~90 ms, results not shown). Furthermore, we observed only a few symmetric [F_6Val^1]gA channels at +300 mV, which indicates that only a small amount of [F_6Val^1]gA had been transferred across the bilayer. Symmetric [F_6Val^1]gA channels should not be dominant, therefore, at negative potentials either—and could not be the events in the lower part of Fig. 6 *B*.

As with [F_6Val^1]/Gly^1]gA channels, [F_6Val^1]/Val^1]gA hybrid channels exhibit transitions between (at least) two current levels. Although there is a suggestion of such behavior in the current traces in Fig. 6 *B*, the existence of multiple conductance states is shown more clearly by an analysis of the duration and interval distributions at both polarities (Fig. 7). At either polarity, the duration histograms for the conducting state can be described by single exponential distributions (Fig. 7, *A* and *C*), indicating the existence of a single type of high-conductance (**H**) state.

The evidence for several dimer states is seen in the **H**-state interval histogram at the negative potential (Fig. 7 *D*), where two components are seen. These components can be interpreted by analogy with the results for [F_6Val^1]/Gly^1]gA channels: the slow component represents leaving the **H** state due to dimer dissociation; and the fast component represents (intraburst) transitions to a "closed" or **L** state. [F_6Val^1]/[Val^1]gA channels thus exhibit current transitions that are qualitatively similar to that observed for [F_6Val^1]/[Gly^1]gA channels.

At positive potentials, the interval histogram (Fig. 7 *B*) is dominated by a slow exponential distribution—the interval between dimers—that is similar to the slow component at negative potentials. The small fast component reflect the presence of very brief transitions (downward in the upper trace of Fig. 6 *B*) from the **H**-state current level to some low-conductance level. These transitions are too short-lived to be resolved, and we cannot reliably determine the current(s) through the low-conductance state(s).

The *i-V* relation for the **H** state of [F_6Val^1]/[Val^1]gA hybrid channels is shown in Fig. 8 and is compared with the *i-V* relations for symmetric [Val^1]gA and [F_6Val^1]gA channels.

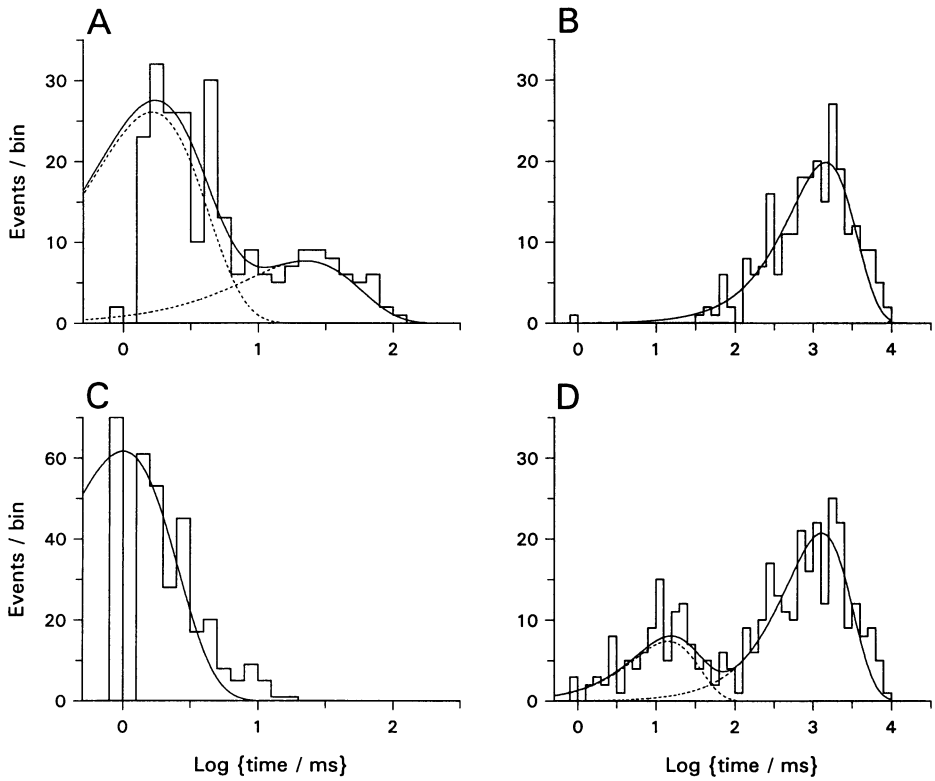

FIGURE 5 Duration distributions for the *hh* events. (*A*) Dimer duration distribution. To determine the dimer durations, the discrimination was set very low, and occasional noise-triggered events were eliminated by manual override. The solid curve shows the least-squares fit obtained when fitting the results by the sum of two exponential distributions; the two interrupted curves show the two distributions. The fast and slow time constants and relative fractions, respectively, are: 1.8 ms and 0.8; and 25 ms and 0.2. (*B*) The corresponding dimer interval distribution. The solid curve shows the least-squares fit obtained when fitting the results by a single exponential distribution. The time constant is 1600 ms. (*C*) Durations of the **H** state only. The solid curve shows the least-squares fit obtained when fitting the results by a single exponential distribution. The time constant is 1.1 ms. (*D*) The corresponding interval distribution. The solid curve shows the least-squares fit obtained when fitting the results by the sum of two exponential distributions; the two interrupted curves show the two distributions. The fast and slow time constants and relative fractions of events, respectively, are: 16 ms and 0.25; and 1400 ms and 0.75.

(We have not been able to resolve a finite current level for the **L** state and do not show results for that state.) The *i-V* relation for the **H** state of [F_6Val^1]/[Val^1]gA hybrid channels is similar to that for the **H** state of the [F_6Val^1]/[Gly^1]gA hybrid channels: current flow in the [F_6Val^1]gA→[Val^1]gA direction is higher than that in the [Val^1]gA→[F_6Val^1]gA direction. The rectification is more pronounced, however: $i(+300)/i(-300) \approx 0.6$, as compared to 0.8 for the **H** state of [F_6Val^1]/[Gly^1]gA channels. At positive potentials the *i-V* relation is below that of symmetric [F_6Val^1]gA channels; at negative potentials the *i-V* relation is superimposed on that for symmetric [F_6Val^1]gA channels. That is why one of the hybrid channel types was missed in the experiments of Russell et al. (1986).

[Ala^1]/[F_6Val^1]gA hybrid channels

Val and Gly residues are very different. We attempted to link these extremes by using Ala as a conceptual bridge. Ala differs from Gly by the substitution of one H at the C_α by a methyl group; chemically, this methyl group makes Ala more similar to Val than to Gly. Correspondingly, [F_6Val^1]/[Ala^1]gA hybrid channels are more similar to [F_6Val^1]/[Val^1]gA than to the [F_6Val^1]/[Gly^1]gA hybrid channels (Fig. 9). When both gramicidin analogs are present at both sides of the bilayer (Fig. 9*A*), one observes the two symmetrical channel types (denoted "F" and "A"), a low-conductance hybrid channel type (denoted *hl*) and brief bursts (denoted *hh*) to a current level that is similar to that for symmetrical [F_6Val^1]gA channels.

As above, the brief events were shown to be hybrid channels in experiments where the two analogs were added asymmetrically (Fig. 9 *B*). At positive potentials one sees the *hl* channels, which show only occasional (and very brief) downward current transitions from an **H** state, and there is no resolved **L** state. At negative potentials one observes the *hh* events, and there are well defined current transitions from an **H** state to a stable "closed" (or **L**) state with a current that is indistinguishable from zero. As was the case with the [F_6Val^1]/[Val^1]gA hybrid channels, the interval histograms have two distinct components (results not shown), where we again interpret the fast component to represent the **L** state durations. At either polarity, the conductance of the **H** state was slightly higher than that of the [F_6Val^1]/[Val^1]gA hybrid channels, and the rectification was even higher ($i(+300)/i(-300) \approx 0.5$).

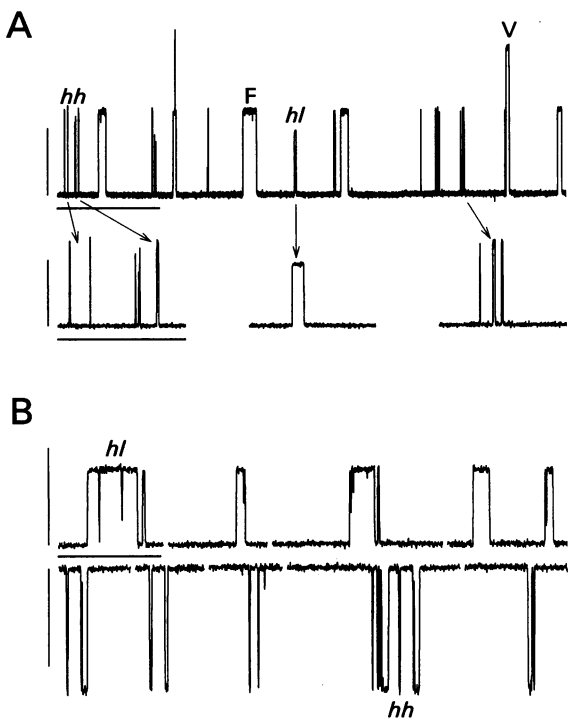

FIGURE 6 [F_6Val^1]/[Val^1]gA hybrid channels. (*A*) Single-channel events observed when both [F_6Val^1]gA and [Val^1]gA are present on both sides of the membrane. Four different channel types can be seen: symmetric [F_6Val^1]gA channels, labeled "F"; symmetric [Val^1]gA channels, labeled "V"; and two hybrid channel events. One type has a current level that is less than that of the [F_6Val^1]gA channels, labeled "*hl*", whereas the other has a bursting appearance to a current level that is similar to that of [F_6Val^1]gA channels, labeled "*hh*." Some of the *hl* and *hh* events are shown at a higher time resolution in the trace segments below the main trace. Calibration bars: vertical 5 pA; horizontal, 2 s (main trace), and 400 ms (trace segments). (*B*) [F_6Val^1]/[Val^1]gA heterodimers at different polarities (sign convention as in Fig. 2). [Val^1]gA was added to the *cis* solution, and [F_6Val^1]gA was added to the *trans* solution. To show the channels' fine structure, only current trace segments are shown. The upper current trace was recorded at +300 mV, one sees *hl* events. The lower current trace was recorded at −300 mV; one sees *hh* events. Calibration bars: vertically, 5 pA; horizontally, 200 ms.

DISCUSSION

Introducing one F_6Val residue asymmetrically at position #1 in only one monomer of a gramicidin A channel produces polarity-dependent conductance transitions in the resulting heterodimeric channels (see also Oiki et al., 1992). We have now established the orientations of the two asymmetric channel types in experiments in which the gramicidins were added asymmetrically, one to each side of a preformed bilayer (cf. O'Connell et al., 1990). Generally, the Xxx→F_6Val substitution brought about three different functional asymmetries: i) polarity-dependent conformational transitions between two different conductance states; ii) polarity-dependent average dimer durations and probabilities of being in the **H** state (at least in [F_6Val^1]/[Gly^1]gA channels); and iii) rectifying *i-V* relations. Asymmetric [F_6Val^1]/[Xxx^1]gA hybrid channels exhibit basic functional similarities to integral membrane protein channels, but with lesser complexity. These channels are suitable for examining conformational transitions in membrane-spanning channels because: i) there exists a consensus structure for the reference [Val^1]gA channel, in which the peptide backbone structure is defined at near-atomic resolution (Arsen'ev et al., 1986; Nicholson and Cross, 1989; Killian et al., 1992; Ketchem et al., 1993); ii) the functional phenotype is caused by a substitution that does not alter the basic channel structure (Durkin et al., 1990); and iii) knowledge about the heterodimer orientation allows for detailed structure-function studies.

[F_6Val^1]/[Gly^1]gA heterodimers exhibit the most clearly resolved gating behavior because of the relatively long residence times in both the **H** and **L** states, and because the **L** state has a finite conductance at both polarities (Fig. 3). The latter finding shows, in itself, that the dimer does *not* dissociate during **H↔L** transitions. Furthermore, the two exponential components in the [F_6Val^1]/[Gly^1]gA dimer duration histograms (Figs. 4 *A* and 5 *A*), together with the existence of two exponential components in the **H** state interval duration histograms (Figs. 4 *D* and 5 *D*), and only one component in the dimer interval distribution (Figs. 4 *B* and 5 *B*), show the existence of (at least) two kinetically distinct states in the dimer. The finite **L** state conductance also permits the determination that the average duration of the [F_6Val^1]/[Gly^1]gA heterodimers and the **H/L** distribution are polarity-dependent. Other [F_6Val^1]/[Xxx^1]gA heterodimers (where Xxx is Ala or Val) display qualitatively similar behavior as the [F_6Val^1]/[Gly^1]gA hybrid channels, but with an **L** state conductance that is indistinguishable from zero. A further dipolar substitution (by a second F_6Val) abolishes this behavior. The polarity-dependent gating behavior is dependent, therefore, upon the single (unpaired) dipolar F_6Val residue.

By itself, the dipole cannot account for all of the results, because F_3Val, which has a dipole moment along the β,γ axis that is similar in magnitude to that of F_6Val in the β,γ,γ' plane (cf. Russell et al., 1986), does *not* induce a similar behavior. Again, although the [F_6Val^1]/[Xxx^1]gA hybrid channels show stronger rectification than other heterodimers with a single dipolar residue at position #1 (e.g., [F_3Val^1]/[Val^1]gA, Russell et al., 1986; and [Met^1]/[Val^1]gA, Andersen et al., 1988), the magnitude of the rectification is difficult to reconcile with the more strongly super-linear *i-V* relations for symmetric [F_3Val^1]gA channels as compared to symmetric [F_6Val^1]gA channels (Russell et al., 1986). This remains a puzzle.

The opposite rectification for the **H** and **L** states (in [F_6Val^1]/[Gly^1]gA channels) suggests that the side chain dipoles are oriented in opposite directions in the two states. Based on the polarity dependence of the **H/L** distribution (see also Oiki et al., 1992), the two CF_3 groups are likely to face away from the [F_6Val^1]gA half of the heterodimer in the **H** state (and be rotated by up to 180° around the C_α-C_β axis to face into the [F_6Val^1]gA monomer in the **L** state). Unfavorable steric interactions between the CF_3 groups and residues in the other monomer would tend to destabilize heterodimers in which either or both of the F_6Val-CF_3

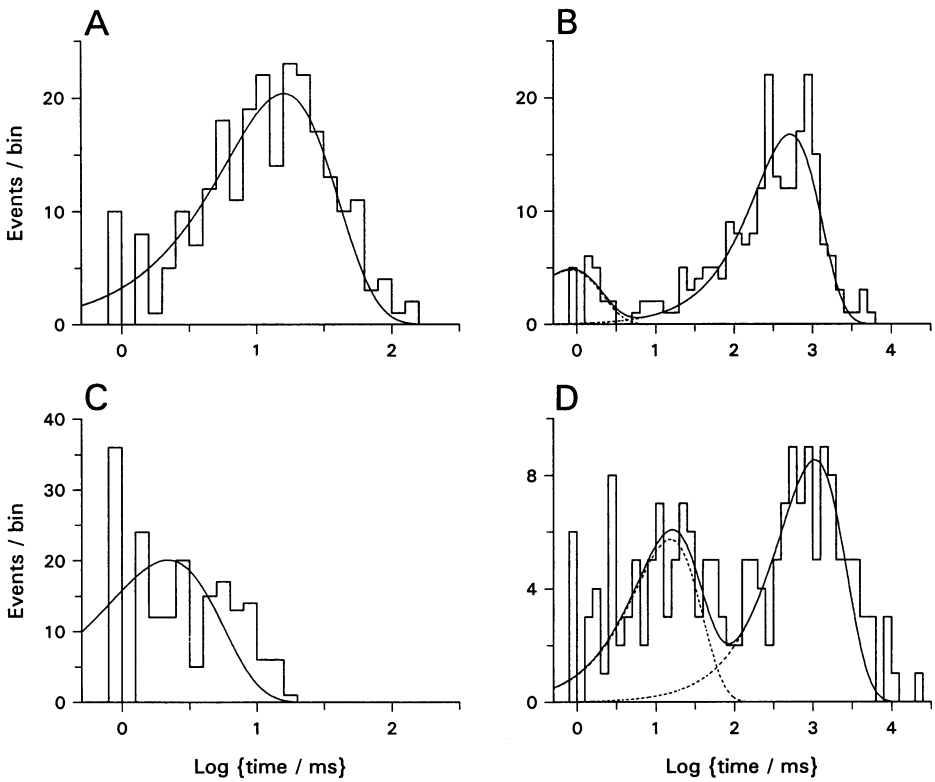

FIGURE 7 Duration distributions for $[F_6Val^1]/[Val^1]gA$ hybrid channels. (*A*) Duration distribution for the **H** state of the *hl* events. The solid curve shows the least-squares fit obtained when fitting the results by a single exponential distribution. The time constant is 18 ms. (*B*) The corresponding dimer interval distribution. The solid curve shows the least-squares fit obtained when fitting the results by the sum of two exponential distributions; the two interrupted curves show the two distributions. The fast and slow time constants and relative fractions, respectively, of events are: 0.9 ms and 0.2; and 580 ms and 0.8. (*C*) Duration distribution for the **H** state of the *hh* events. The solid curve shows the least-squares fit obtained when fitting the results by a single exponential distribution. The time constant is 2.4 ms. (*D*) The corresponding interval distribution. The solid curve shows the least-squares fit obtained when fitting the results by the sum of two exponential distributions; the two interrupted curves show the two distributions. The slow and fast time constants and relative fractions, respectively, of events are: 17 ms and 0.4; and 1200 ms and 0.6.

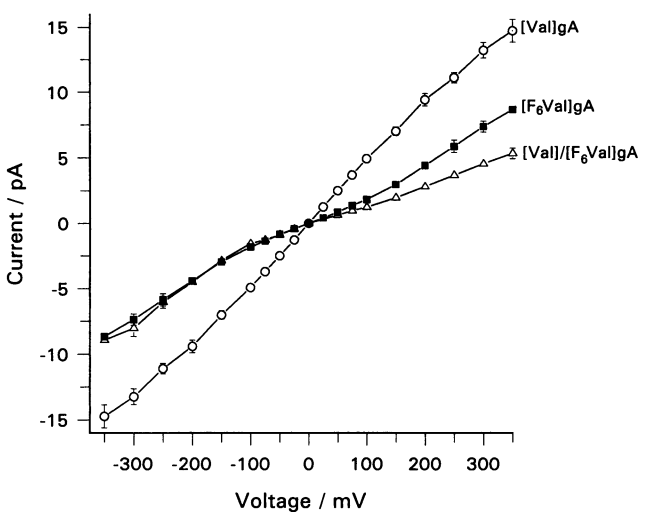

FIGURE 8 Single-channel *i-V* relation for symmetric $[F_6Val^1]gA$ and $[Val^1]gA$ channels and for $[F_6Val^1]/[Val^1]gA$ heterodimers. Mean ± SD (where larger than the symbol). Symbols: ■, symmetric $[Val^1]gA$ channels; △, symmetric $[F_6Val^1]gA$ channels; ○, $[Val^1]/[F_6Val^1]gA$ channels.

groups face toward the $[Xxx^1]gA$ monomer, and the polarity-dependent dimer durations (Fig. 3) are consistent with the proposed arrangement. A plausible mechanistic role for the dipole is that the **L**↔**H** conformational change is initiated by an electric field-induced reorientation of the F_6Val residue in the heterodimer—and that the side chain reorientation drives a more global conformational change.

The argument for more global conformational changes is based, in part, on energetic considerations. At 300 mV, for example (when the electric field, E, is $\sim 1.2 \cdot 10^8$ V/m), the maximal side rotation (180°) around the C_α-C_β axis (from an alignment with the field to an alignment against the field) would give rise to an electrostatic energy difference ($2 \cdot \vec{\mu} \cdot V$, where $\vec{\mu}$ is the dipole moment in the β,γ,γ' plane, ~1.6 Debye) that is only ~0.8 kJ/mol or ~0.2 kT at 25°C. Assuming a two-state gating model, the field-driven side-chain reorientation can only account for ~50% of the change in $p_H(V)$ between −300 and +300 mV (see also Oiki et al., 1992). Another indication of more extensive conformational changes (in a "stable" dimer) is that the **H**↔**L** transitions depend on the identity of the formyl-NH-terminal residue in the *other* monomer; the conductance of the **L** state in $[F_6Val^1]/[Gly^1]gA$ heterodimers is finite, whereas it is indistinguishable from zero in $[F_6Val^1]/[Val^1]gA$ and $[F_6Val^1]/[Ala^1]gA$ heterodimers. Mechanistically, a field-induced rotation of the F_6Val side chain could distort the peptide backbone, and thereby trigger more extensive changes in the dimer structure that lead to the reduction of the conductance (or channel closure).

$[F_6Val^1]/[Ala^1]gA$ heterodimers are more similar to the $[F_6Val^1]/[Val^1]gA$ than to the $[F_6Val^1]/[Gly^1]gA$ heterodimers, in the sense that a "stable" **L** state conductance is observed only in the $[F_6Val^1]/[Gly^1]gA$ channels. The increased backbone flexibility that is imparted by the Gly^1 residue (cf. Schulz and Schirmer, 1979) thus seems to be causally related to having a finite **L** state conductance. The increased rigidity that is imparted by having a β-branched (Val), as

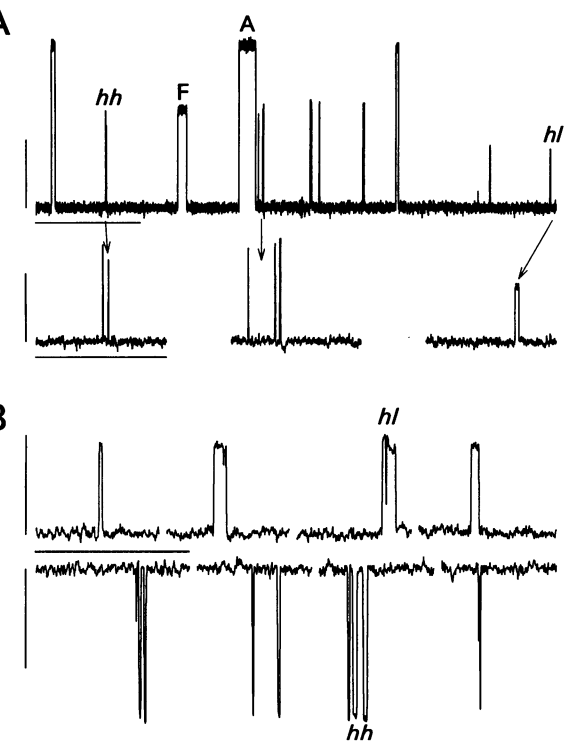

FIGURE 9 [F_6Val^1]/[Ala^1]gA hybrid channels. (*A*) Single-channel events observed when both [F_6Val^1]gA and [Ala^1]gA are present on both sides of the membrane. Four different channel types can be seen: symmetric [F_6Val^1]gA channels, labeled "F"; symmetric [Ala^1]gA channels, labeled "A"; and two hybrid channel events. One type has a current level that is less than that of the [F_6Val^1]gA channels, labeled "*hl*," whereas the other has a bursting appearance to a current level that is similar to that of [F_6Val^1]gA channels, labeled "*hh*." Some of the *hl* and *hh* events are shown at a higher time resolution in the trace segments below the main trace. Calibration bars: vertical 5 pA; horizontal, 2 s (main trace), and 400 ms (trace segments). (*B*) [F_6Val^1]/[Ala^1]gA heterodimers at different polarities (sign convention as in Fig. 2). [Ala^1]gA was added to the *cis* solution, and [F_6Val^1]gA was added to the *trans* solution. To show the channels' fine structure, only current trace segments are shown. The upper current trace was recorded at +300 mV; one sees *hl* events. The lower current trace was recorded at −300 mV; one sees *hh* events. Calibration bars: vertically, 5 pA; horizontally, 200 ms.

contrasted with a straight-chain (Ala) residue at position 1, seems to have only a modest effect.

In gramicidin channels the side chains do not contact the permeating ions directly. Nonpolar side-chain replacements, therefore, alter the energy profile for ion movement primarily by means of steric backbone perturbations, and single-channel recordings provide an ultrasensitive detector of the backbone conformational changes. The quantitative differences that are seen when having Val, Ala, or Gly residues in [F_6Val^1]/[Xxx^1]gA heterodimers, for example, are likely to be expressions of altered backbone flexibility due to the different side-chain geometries. It is in this respect intriguing that a Leu→Val substitution, which exchanges a γ-branched- with a β-branched residue, in the S5-S6 linker (or P segment) of a chimeric (Kv3.1/Kv2.1) voltage-dependent potassium channel alters both ion selectivity (Kirsch et al., 1992) and channel gating (Taglialatela et al., 1992). The S5-S6 linker is believed to form (part of) the pore for K^+ permeation and to have a β-structure (e.g., Bogusz and Busath, 1992; Durell and Guy, 1992). The conductance transitions that we have described here may be relevant for understanding the pore region of polarity-dependent channels.

We thank M. D. Becker, D. B. Sawyer, and G. Saberwal for helpful discussion.

This work was supported by National Institutes of Health grants GM21342 and GM34968.

REFERENCES

Andersen, O. S. 1983. Ion movement through gramicidin A channels. Single-channel measurements at very high potentials. *Biophys. J.* 41: 119–133.

Andersen, O. S., J. T. Durkin, and R. E. Koeppe II. 1988. Do amino acid substitutions alter the structure of gramicidin channels? Chemistry at the single molecule level. *Jerusalem Symp. Quant. Chem. Biochem.* 21: 115–132.

Andersen, O. S., and R. E. Koeppe II. 1992. Molecular determinants of channel function. *Physiol. Rev.* 72:S89–S158.

Andersen, O. S., D. B. Sawyer, and R. E. Koeppe II. 1992. Modulation of channel function by the host bilayer. *In* Biomembrane Structure and Function. B. P. Gaber and K. R. K. Easwaran, editors. Adenine Press, Schenectady, NY. 227–244.

Apell, H.-J., E. Bamberg, H. Alpes, and P. Läuger. 1977. Formation of ion channels by a negatively charged analog of gramicidin A. *J. Membr. Biol.* 31:171–188.

Arsen'ev, A. S., A. L. Lomize, I. L. Barsukov, and V. F. Bystrov. 1986. Gramicidin A transmembrane ion-channel. Three-dimensional structure reconstruction based on NMR spectroscopy and energy refinement. *Biol. Membr.* 3:1077–1104.

Becker, M. D., D. V. Greathouse, R. E. Koeppe II, and O. S. Andersen. 1991. Amino acid sequence modulation of gramicidin channel function. Effects of tryptophan-to-phenylalanine substitutions on the single-channel conductance and duration. *Biochemistry.* 30:8830–8839.

Bogusz, S., and D. Busath. 1992. Is a β-barrel model of the K^+ channel energetically feasible? *Biophys. J.* 62:19–21.

Busath, D. D. 1993. The use of physical methods in determining gramicidin channel structure and function. *Annu. Rev. Physiol.* 55:473–501.

Durell, S. R., and H. R. Guy. 1992. Atomic scale structure and function models of voltage-gated potassium channels. *Biophys. J.* 62:238–250.

Durkin, J. T., R. E. Koeppe II, and O. S. Andersen. 1990. Energetics of gramicidin hybrid channel formation as a test for structural equivalence. Side-chain substitutions in the native sequence. *J. Mol. Biol.* 211: 221–234.

Fonseca, V., P. Daumas, L. Ranjalahy-Rasoloarijao, F. Heitz, R. Lazaro, Y. Trudelle, and O. S. Andersen. 1992. Gramicidin channels that have no tryptophan residues. *Biochemistry.* 31:5340–5350.

Ketchem, R. R., W. Hu, and T. A. Cross. 1993. High-resolution conformation of gramicidin A in a lipid bilayer by solid state-state NMR. *Science.* 261:1457–1460.

Killian, J. A. 1992. Gramicidin and gramicidin-lipid interactions. *Biochim. Biophys. Acta.* 1113:391–425.

Killian, J. A., M. J. Taylor, and R. E. Koeppe II. 1992. Orientation of the valine-1 side chain of the gramicidin transmembrane channel and implications for channel functioning. A ^{2}H NMR study. *Biochemistry.* 31: 11283–11290.

Kirsch, G. E., J. A. Drewe, M. Taglialatela, R. H. Joho, M. DeBiasi, H. A. Hartmann, and A. M. Brown. 1992. A single nonpolar residue in the deep pore of related K+ channels acts as a K^+:Rb^+ conductance switch. *Biophys. J.* 62:136–144.

Koeppe, R. E., II, L. L. Providence, D. V. Greathouse, F. Heitz, Y. Trudelle, N. Purdie, and O. S. Andersen. 1992. On the helix sense of gramicidin A single channels. *Proteins.* 12:49–62.

Mazet, J. L., O. S. Andersen, and R. E. Koeppe, II. 1984. Single-channel studies on linear gramicidins with altered amino acid sequences. A comparison of phenylalanine, tryptophan, and tyrosine substitutions at positions 1 and 11. *Biophys. J.* 45:263–276.

Nicholson, L. K., and T. A. Cross. 1989. Gramicidin cation channel: an experimental determination of the right-handed helix sense and verification of β-type hydrogen bonding. *Biochemistry.* 28:9379–9385.

O'Connell, A. M., R. E. Koeppe II, and O. S. Andersen. 1990. Kinetics of gramicidin channel formation in lipid bilayers: transmembrane monomer association. *Science.* 250:1256–1259.

Oiki, S., R. E. Koeppe II, and O. S. Andersen. 1992. A dipolar amino acid substitution induces voltage-dependent transitions between two stable conductance states in gramicidin channels. *Biophys. J.* 62:28–30.

Russell, E. W. B., L. B. Weiss, F. I. Navetta, R. E. Koeppe II, and O. S. Andersen. 1986. Single-channel studies on linear gramicidins with altered amino acid side chains. Effects of altering the polarity of the side chain at position 1 in gramicidin A. *Biophys. J.* 49:673–686.

Sarges, R., and B. Witkop. 1965. Gramicidin A. V. The structure of valine- and isoleucine-gramicidin A. *J. Am. Chem. Soc.* 87:2011–2019.

Schulz, G. E., and R. H. Schirmer. 1979. Principles of Protein Structure. Springer-Verlag, New York.

Sigworth, F. J., and S. M. Sine. 1987. Data transformations for improved display and fitting of single-channel dwell time histograms. *Biophys. J.* 52:1047–1054.

Taglialatela, M., G. E. Kirsch, A. M. J. VanDongen, J. A. Drewe, H. A. Hartmann, R. H. Joho, E. Stefani, and A. M. Brown. 1992. Gating currents from a delayed rectifier K^+ channel with altered pore structure and function. *Biophys. J.* 62:34–36.

Veatch, W., and L. Stryer. 1977. The dimeric nature of the gramicidin A transmembrane channel: conductance and fluorescence energy transfer studies of hybrid channels. *J. Mol. Biol.* 113:89–102.

Weiss, L. B., and R. E. Koeppe II. 1985. Semisynthesis of linear gramicidins using diphenyl phosphorazidate (DPPA). *Int. J. Pept. Protein Res.* 26: 305–310.